*Advances in River Sediment Research – Fukuoka et al. (eds)*
*© 2013 Taylor & Francis Group, London, ISBN 978-1-138-00062-9*

# Numerical analysis of flood flows and bed variations at river confluences of the Go River

Y. Takemura & S. Fukuoka
*Research and Development Initiative, Chuo University, Kasuga, Bunkyo Word, Tokyo, Japan*

ABSTRACT: In confluences of rivers having a comparable drainage area, a strong mixing of a mainstream and tributaries flows which have a large momentum in a different direction induces complex three-dimensional flow structures. In this study, the Bottom Velocity Computation (BVC) method consist of shallow water equations, depth-integral vorticity equations and water surface velocity equations was extended by introducing the flux integral method considering a non-orthogonal direction of a grid line for properly evaluating flood flows and bed variations in the confluences. The extended model was applied to recent large floods in the Go River confluences to investigate the flood flows and bed variations during the flood events. From the calculation results, we clarified that separation zones formed at the confluences have pronounced effects on the three-dimensional flow structure and bed variations for the downstream channel.

## 1 INTRODUCTION

The confluences of the Go River, Basen River and Saijyo River are located in the Chugoku district, Japan. Each river has a comparable drainage area, and the Basen River joins the Go River with a great curvature at immediately downstream from the junction of the Basen River and Saijyo River as shown in Figure 1. In such river confluences, a strong mixing of the mainstream and tributaries flows which have a large momentum in a different direction induces complex three-dimensional flow structures. Flood flows and bed variations at the confluences are great concern of river engineers.

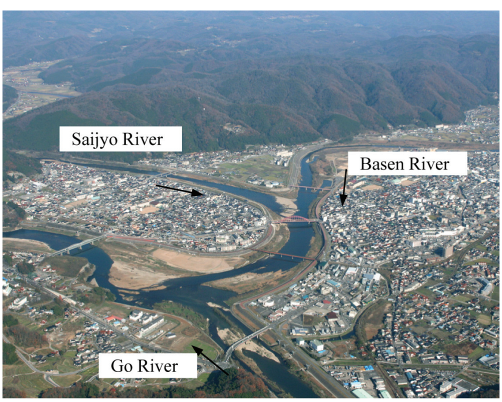


Figure 1. Air photograph of the Go River confluences (Sep. 2006).

Recently, full 3D turbulence model comes to be used for investigating the three-dimensional flow structures at river confluences (Miyawaki et al. 2010). But because the flow structures and sediment transport at the confluences are also affected by spatial and temporal large scale flows, more practical numerical model capable of evaluating the confluence flows and bed variations is required.

In the case where the depth of a confluence area is shallow, it is expected that three-dimensional flows induced by deflections of depth-average flows dominates in the flow structures and bed variations. Recently, Uchida & Fukuoka (2011) proposed the Bottom Velocity Computation (BVC) method consist of shallow water equations, depth-integral vorticity equations and water surface velocity equations. Because the BVC method is based on the shallow water model, three-dimensional flows and corresponding sediment transports can be calculated more reasonably than the full 3-D turbulence model. On the other hand, since transports and deformations of the depth-integral vorticity are restricted by the depth-average flow fields, the computation accuracy of the depth-average velocity directly affects the resulting calculated three-dimensional flow structures and bed variations. As reported in previous studies, when the convection terms in the momentum equations are approximated using upwind difference scheme, a large error may result in the flow where the grid line and flow directions are not closely aligned (Rhie & Chow 1983, Leonard et al. 1994). This influence would be more pronounced in the confluences.

In this study, we developed the flux integral method considering a non-orthogonal direction of a grid line based on the CIP-CSL scheme (Nakamura et al. 2001) for evaluating the convection terms more accurately also in the complex flow fields of the confluences and it was combined with the BVC method. The developed model was applied to recent large floods in October 1998 and June 1999 at the Go river confluences to investigate the flood flows and bed variations during the flood events.

## 2 COMPUTATIONAL METHOD

### 2.1 *Framework of computational method*

Figure 2 shows framework of the computational method of this study. The governing equations of the Bottom Velocity Computation (BVC) method, i.e. shallow water equations, depth-integral vorticity equations and surface velocity equations (Uchida & Fukuoka 2011), are discretized on a non-orthogonal grid to properly evaluate complex boundaries of river confluences. In the BVC method, vertical distributions of horizontal velocity components are approximated by a cubic function, and it allows calculating the momentum exchange due to the vertical distribution of the velocity.

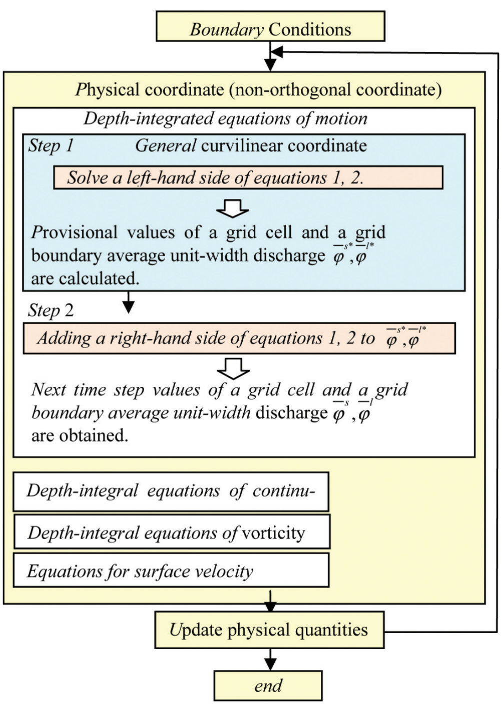


Figure 2. Framework of computation method.

Since the convection terms of the depth-integral equations of motion are calculated based on the CIP-CSL scheme (Nakamura et al. 2001), the grid cell and grid boundary average unit-width discharge are solved by following equations:

$$\frac{\partial \overline{\varphi}^{s}}{\partial t} + \frac{1}{S}\left( Flux_e - Flux_w + Flux_n - Flux_s \right) = \overline{D}^{s} \quad (1)$$

$$\frac{\partial \overline{\varphi}^{l}}{\partial t} + \overline{U}^{l}\frac{\partial \overline{\varphi}^{l}}{\partial x} + \overline{V}^{l}\frac{\partial \overline{\varphi}^{l}}{\partial y} = -\overline{\varphi}^{l}\left(\frac{\partial \overline{U}^{l}}{\partial x} + \frac{\partial \overline{V}^{l}}{\partial y}\right) + \overline{D}^{l} \quad (2)$$

$$D = \begin{cases} -gh\dfrac{\partial z_s}{\partial x} - \dfrac{\tau_{bx}}{\rho} + \dfrac{h}{\rho}\left(\dfrac{\partial \tau_{xx}}{\partial x} + \dfrac{\partial \tau_{xy}}{\partial y}\right) - \dfrac{F_x}{\rho} \\ -gh\dfrac{\partial z_s}{\partial y} - \dfrac{\tau_{by}}{\rho} + \dfrac{h}{\rho}\left(\dfrac{\partial \tau_{yx}}{\partial x} + \dfrac{\partial \tau_{yy}}{\partial y}\right) - \dfrac{F_y}{\rho} \end{cases} \quad (3)$$

where $\varphi$ (=$Uh$, $Vh$) = unit-width discharge components in $x$ and $y$ directions; $U$, $V$ = depth-average velocity components in $x$ and $y$ directions; $h$ = water depth; $\rho$ = fluid density; $g$ = the acceleration of gravity; $Flux_{e,w,n,s}$ = momentum flux from grid boundaries $e$, $w$, $n$ and $s$ shown in Figure 3. Here, overbars "–s" and "–l" indicate a grid cell and a grid boundary

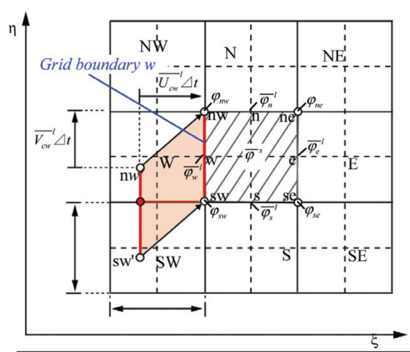


*Interpolation* function for distribution of unit-width discharge components $\varphi$ within each grid cell

$$\varphi_{i,j}\left(\tilde{\xi},\tilde{\eta}\right) = c_0 + c_1\tilde{\xi} + c_2\tilde{\xi}^2 + c_3\tilde{\eta} + c_4\tilde{\eta}^2 + c_5\tilde{\xi}\tilde{\eta} + c_6\tilde{\xi}^2\tilde{\eta} + c_7\tilde{\xi}\tilde{\eta}^2 + c_8\tilde{\xi}^2\tilde{\eta}^2$$

$$c_0 = \phi_{sw} \quad c_1 = -4\phi_{sw} - 2\phi_{se} + 6\overline{\phi}^{l}_{s} \quad c_2 = 3\phi_{se} + 3\phi_{sw} - 6\overline{\phi}^{l}_{s}$$

$$c_3 = -4\phi_{sw} - 2\phi_{nw} + 6\overline{\phi}^{l}_{w} \quad c_4 = 3\phi_{nw} + 3\phi_{sw} - 6\overline{\phi}^{l}_{w}$$

$$c_5 = 16\phi_{sw} + 8\phi_{se} + 8\phi_{nw} + 4\phi_{ne} - 12\left(\overline{\phi}^{l}_{n} + 2\overline{\phi}^{l}_{s}\right) - 12\left(\overline{\phi}^{l}_{e} + 2\overline{\phi}^{l}_{w}\right) + 36\overline{\phi}^{s}$$

$$c_6 = -12\phi_{sw} - 12\phi_{se} - 6\phi_{nw} - 6\phi_{ne} + 12\left(\overline{\phi}^{l}_{n} + 2\overline{\phi}^{l}_{s}\right) + 18\left(\overline{\phi}^{l}_{e} + \overline{\phi}^{l}_{w}\right) - 36\overline{\phi}^{s}$$

$$c_7 = -12\phi_{sw} - 6\phi_{se} - 12\phi_{nw} - 6\phi_{ne} + 18\left(\overline{\phi}^{l}_{n} + \overline{\phi}^{l}_{s}\right) + 12\left(\overline{\phi}^{l}_{e} + 2\overline{\phi}^{l}_{w}\right) - 36\overline{\phi}^{s}$$

$$c_8 = 9\phi_{sw} + 9\phi_{se} + 9\phi_{nw} + 9\phi_{ne} - 18\left(\overline{\phi}^{l}_{n} + \overline{\phi}^{l}_{s}\right) - 18\left(\overline{\phi}^{l}_{e} + \overline{\phi}^{l}_{w}\right) + 36\overline{\phi}^{s}$$

$$\tilde{\xi} = (\xi - \xi_{sw})/\Delta\xi \qquad \tilde{\eta} = (\eta - \eta_{sw})/\Delta\eta$$

Figure 3. Arrangements of variables and interpolation function for unit-width discharge distribution within a grid cell.

average value, respectively. Bed shear stresses $\tau_{bx,y}$ and vegetation resistances $F_{x,y}$ are given as:

$$\tau_{bx} = \rho c_b u_b \sqrt{u_b^2 + v_b^2}, \; \tau_{by} = \rho c_b v_b \sqrt{u_b^2 + v_b^2} \tag{4}$$

$$F_x = \frac{\rho g h_a}{K} U \sqrt{U^2 + V^2}, \; F_y = \frac{\rho g h_a}{K} V \sqrt{U^2 + V^2} \tag{5}$$

where $u_b$, $v_b$ = bottom velocity components in $x$ and $y$ directions; $K$ = vegetation permeability coefficient; $h_a$ = height of a tree. $c_b$ is defined by the relationship with the equivalent roughness $k_s$:

$$c_b = Ar + \frac{1}{\kappa} \ln\left(\frac{z_b}{k_s}\right) \tag{6}$$

where $Ar = 8.5$; $\kappa = 0.4$; $z_b = \delta z_b + k_s$; $\delta z_b = h/(e^3 - 1)$. In this study, $k_s$ is given as follows:

$$k_s = (n/0.0417)^6 \tag{7}$$

where $n$ = the Manning's roughness coefficient. $\tau_{xx}$, $\tau_{xy}$, $\tau_{yy}$, $\tau_{yx}$ are the horizontal shear stresses consist of the momentum exchange due to the turbulence and vertical distribution of horizontal velocity and they are written as follows:

$$\begin{aligned} \tau_{xx} &= 2\nu_t \frac{\partial u}{\partial x} + \overline{u'u'} \\ \tau_{xy}, \tau_{yx} &= \nu_t \left(\frac{\partial v}{\partial x} + \frac{\partial u}{\partial y}\right) + \overline{u'v'} \\ \tau_{yy} &= 2\nu_t \frac{\partial v}{\partial y} + \overline{v'v'} \end{aligned} \tag{8}$$

where $\nu_t$ = depth-average turbulent viscosity; $u', v'$ = deviation velocity components from depth-average velocity in $x$ and $y$ directions. $\nu_t$ is calculated from equivalent condition of the turbulent kinetic energy at each point. Here, overbar "–" indicates a depth-average value.

Equations 1, 2 are solved in two steps. The first step is to solve provisional values $\overline{\varphi}^{s*}$ and $\overline{\varphi}^{l*}$ from the equations without considering a right-hand side of the equations (details are discussed in 2.2). The second step is to correct the provisional values by considering a right-hand side of the equations. Through these steps, the values of $\overline{\varphi}^{s}$ and $\overline{\varphi}^{l}$ of next time step are obtained.

### 2.2 *Computation method for convection terms*

To calculate the convection terms of the depth-integral equations of motion accurately, the CIP_CSL method is introduced. The two-dimensional CIP_CSL methods have been proposed by researchers (Takizawa & Yabe 2000, Nakamura et al. 2001). But because these methods were proposed on an orthogonal grid, applications to the engineering problems were limited. In this study, a calculation method of the convection terms on a non-orthogonal grid will be developed based on the CIP_CSL method.

Figure 3 shows the arrangements of the variables used for the calculation of the convective terms. In this model, distribution of $\varphi$ within each grid cell is approximated by a two-dimensional quadratic polynomial shown in Figure 3. 9 constants included in the quadratic polynomial $c_{0\text{–}8}$ are determined from a grid point values, a grid boundary average values and a grid cell average value of $\varphi$ at each grid cell (see Fig. 3). Here, the grid point values are interpolated from the grid boundary average values for the advantage of the computation efficiency in this study. A calculation method for $\overline{\varphi}^{l}$ and momentum flux at the gird boundary $w$ is shown below as an example. First, upstream points $nw'$ and $sw'$ described in Figure 3 are calculated from contravariant components of a depth-average velocity $\overline{\varphi}^{l}$ at grid boundary $w$ $\overline{U_{cw}}^{l}$, $\overline{V_{cw}}^{l}$ and the time step $\Delta t$ in the general curvilinear coordinate. The provisional value $\overline{\varphi}^{l*}$ is obtained as the integral of the interpolation function of $\varphi$ in grid cell $W$ from $nw'$ to $sw'$. The momentum flux from the grid boundary $w$ are also calculated by adding the integrals of the interpolation function in grid cell $W$ throughout the area surrounded by $nw$, $nw'$, $sw$, $p$ and of the interpolation function in grid cell $SW$ throughout the area surrounded by $sw'$, $sw$, $p$. $\overline{\varphi}^{l*}$ and the momentum flux at each grid boundary is calculated in the same manner. And the provisional value $\overline{\varphi}^{S*}$ of each grid cell is calculated from the budget of the momentum flux from the grid boundaries $e$, $w$, $n$ and $s$.

## 3 APPLICATION TO THE GO RIVER CONFLUENCES

Figure 4 shows the plane form and observation stations in the Go River confluences. The bed topography at the confluence consisted large bars, and the excessive grows of vegetations and sedimentation have been essential problems. In this area, large floods occurred at October 1998 and June 1999 and flood data were obtained. We apply the model constructed in preceding chapter to these floods for investigating applicability of the model and characteristics of flood flows and sediment transports at the confluences.

### 3.1 *Computation conditions*

Observed water level hydrographs at Awaya (141.6 km point of the Go River), Minamihatashiki

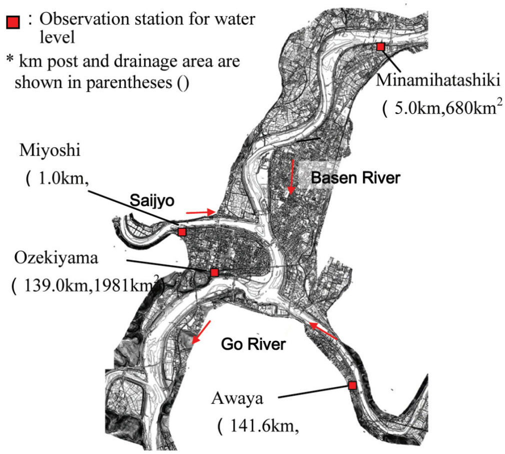


Figure 4. Plane form and observation stations in the Go River confluences.

Table 1. The Manning's roughness coefficient and vegetation permeability confident of calculated area.

| | Roughness coefficient ($m^{-1/3} \cdot s$) |
|---|---|
| Go River (main channel) | 0.032 |
| Go River (flood plain) | 0.042 |
| Basen River (main channel) | 0.032 |
| Basen River (flood plain) | 0.045 |
| Saijyo River (main channel) | 0.032 |
| Saijyo River (flood plain) | 0.042 |

*Vegetation permeability coefficients are given in the range from 30 to 50 at the vegetated areas.

(5.0 km point of the Basen River) and Miyoshi (1.0 km point of the Saijyo River) observation stations are given as upstream boundary conditions of each river instead of discharge hydrographs. Downstream boundary condition is given by a observed water level hydrograph at Ozekiyama observation station (139.0 km point of the Go River). The Manning's roughness coefficient and vegetation permeability coefficient of calculated area are determined by reference to the previous study (Fukuoka et al. 2007) as shown in Table 1.

Figure 5 is grain size distributions of the each river. Significant difference cannot be found among them. We give the grain size distributions indicated by plots to each river uniformly throughout river reach for the calculation. In the calculation of sediment transport, bed load with 8 grain size groups ranging between 0.3 and 1.25 mm was considered. The bed load transport rate of each grain size is calculated by Ashida & Michiue formula (1972). The change in the river bed elevation and

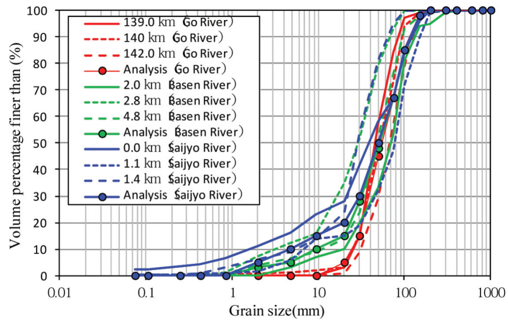


Figure 5. Grain size distributions in the Go River confluences.

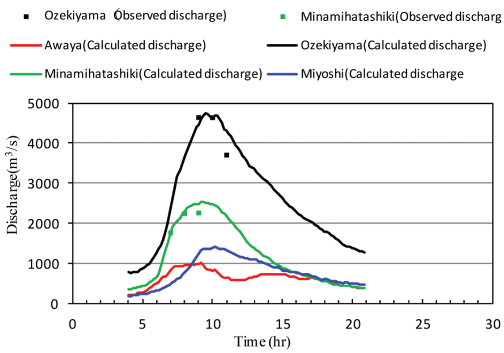


(a) Oct. 1998 flood.

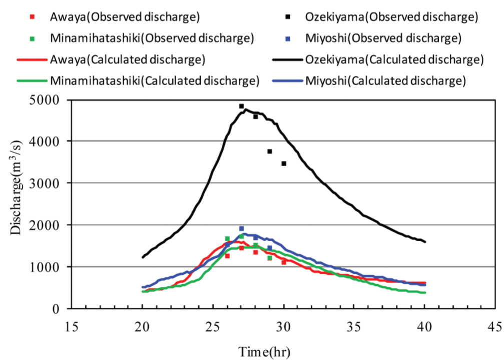


(b) Jun. 1999 flood.

Figure 6. Comparison between observed and calculated discharge hydrographs of Oct. 1998 and Jun. 1999 floods.

fraction of the materials in surface layer are calculated by using Hirano equations (1971).

### 3.2 *Computational results*

Figures 6a, b are comparison between the observed and calculated discharge hydrographs of the

1998 and 1999 floods at the observation stations. Although the calculated discharge hydrographs tend to be large compared with the observed discharge in the deciding period at Ozekiyama observation station (139 km point of the Go River), they show good agreement in the both floods. Figure 7 shows longitudinal distributions of the calculated maximum water levels and flood marks of the 1998 and 1999 floods. Although the calculated maximum water levels almost reflect the height of the flood marks, the difference between the calculated maximum water levels and flood marks becomes large in the upstream reach of 2.0 km point of the Basen River. The main reason is considered below. The Manning's equation is used for resistance to flow in relatively low vegetation and the roughness coefficient is given uniformly for flood plains in each river in this study. As shown in Figure 5, the Basen River has relatively large flood plains, and distribution of the vegetation covering flood plains should not be neglected for the resistant to flow.

### 3.3 *Consideration for characteristics of flood flows and bed variations in the Go River confluences*

Characteristics of flood flows and bed variations in the Go River confluences are investigated based on the observed data and calculation results. Figures 8a, b show calculated 10 minutes average

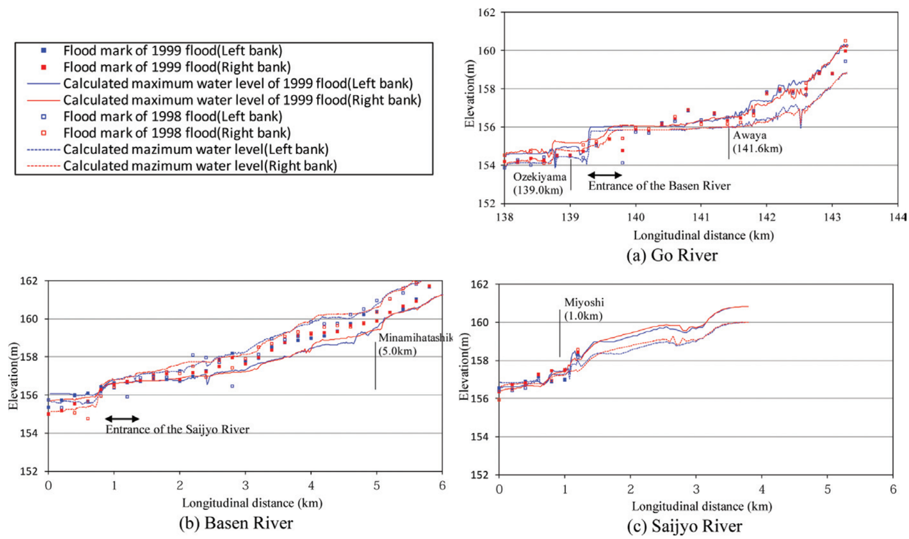


Figure 7. Comparison between the longitudinal distributions of the calculated maximum water levels and flood marks in the 1998 and 1999 floods.

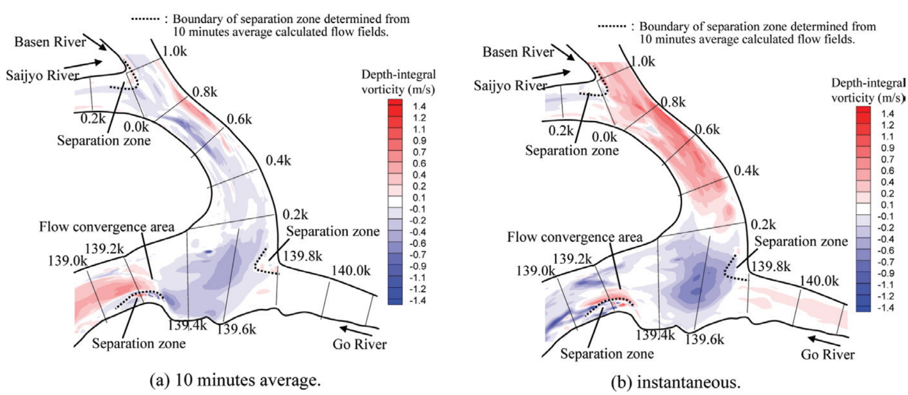


Figure 8. Comparison of distributions of 10 minutes average and instantaneous depth-integral vorticity in the direction of depth-average velocity at peak of the 1998 flood.

and instantaneous distribution of depth-integral vorticity in the direction of the depth-average velocity in the peak of the 1998 flood when the bed variations were occurred most. Red color corresponds to the positive vorticity (counter-clockwise rotation) and blue color indicates the negative vorticity (clockwise rotation). The instantaneous vorticity distribution is quite different from the 10 minutes average vorticity distribution, especially at the downstream of the junction of the Basen River and Saijyo River and the flow convergence area around 139.2 km point of the Go River, because of the unsteady vortex motion at the separation zones surrounded by black broken line in Figure 8. In addition, the clockwise depth-integral vorticity (indicated in blue color) formed at the downstream reach of the junction of the Basen River and Saijyo River is transported to the flow convergence area around 139.2 km point of the Go River at the peak of the 1998 flood.

Figures 9a, b show the observed and calculated bed variation contour before and after the 1998 and 1999 floods. As shown in Figure 9a, deposition and bed scouring were occurred mainly at the junction of the Basen River and Saijyo River and around the flow convergence area around 139.2 km point of the Go River. The calculated bed variations shown in Figure 9b can reproduce the bed scouring along the flow convergence area, but the scouring area is short in a longitudinal direction and wide in a transverse direction compared with the observed data shown by Figure 9a. In addition, the calculated bed variations cannot fully reproduce the depositions at the junction of the Basen River and Saijyo River.

### 3.4 *Consideration for effects of the momentum flux of a non-orthogonal direction of a grid line*

The key feature of the proposed model is considering the momentum flux of a non-orthogonal direction of a grid line in the calculation of the convection terms. Therefore, the calculation without considering the momentum flux of a non-orthogonal direction of a grid line (Run-2) is conducted under the same conditions as in the calculation of the preceding section (Run-1) to examine the applicability of the proposed model.

Figure 10 shows the calculated bed variation contour before and after the 1998 and 1999 floods by Run-2. It can be seen that the calculated bed variations of Run-1 (Fig. 9b) and Run-2 (Fig. 10) indicate different features at the downstream of the flow convergence area around 139.2 km point of the Go River (139.2–139.0 km reach), and the calculation result of Run-1 comes closer to the observed results indicated by Figure 9a than the result of Run-2.

Next, trajectories of the water particles at vicinity of the water surface and river bed in the peak of the 1998 flood are compared between Run-1 and Run-2 in Figure 11. The trajectories are estimated from 10 minutes average calculated surface velocities and bottom velocities. The trajectories at the vicinity of water surface assume a case observers toss floating rods into the channel from the Kotobuki and Tomoe Bridge shown in Figure 11. The trajectories at the vicinity of river bed are described by focusing on the motion of the particles around the flow convergence area around 139.2 km. The discrepancy of the trajectories at vicinity of the water surface between Run-1 and Run-2 becomes large at the junction of the Go River and Basen River and downstream of the flow convergence area (see Fig. 11a). And the water particles at the vicinity of river bed toward the left bank in the downstream of the flow convergence area in Run-1 compared with Run-2. It would be considered as the main cause of the difference of the calculated bed variations between Figure 9b and Figure 10 in the downstream of the flow convergence area.

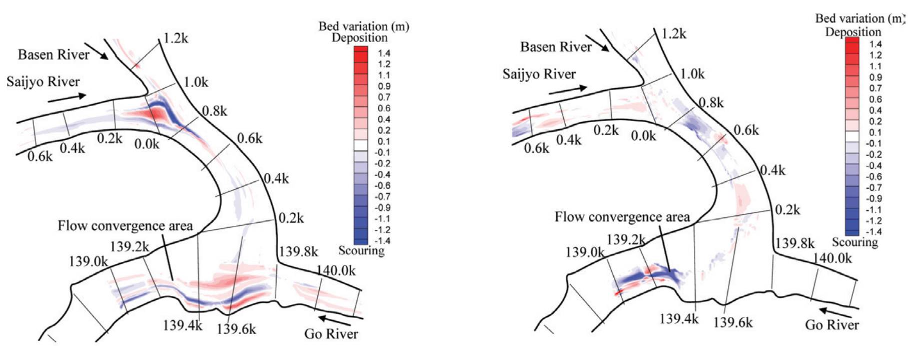


(a) Observation. (b) Calculation.

Figure 9. Comparison between the observed and calculated bed variation contour before and after the 1998 and 1999 floods.

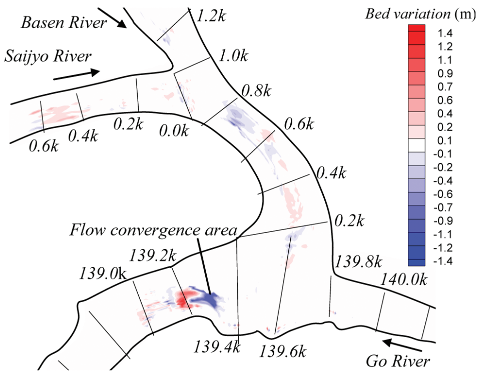


Figure 10. Calculated bed variation contour before and after the 1998 and 1999 floods (without considering a non-orthogonal direction of a grid line in the calculation of convection terms).

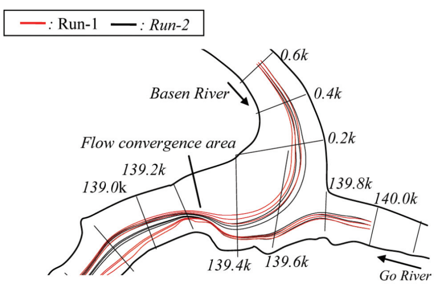


*(a) Trajectories of water particles* at vicinity of water surface.

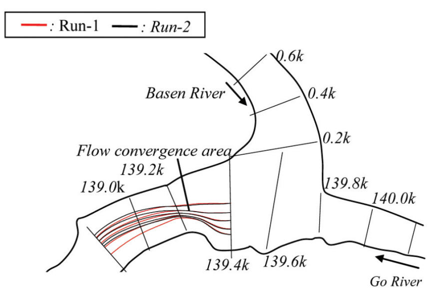


(b) Trajectories of water particles at vicinity of river bed.

Figure 11. Calculated trajectories of water particles at vicinity of water surface and river bed at the peak of the 1998 flood in Run-1 and Run-2.

Although the applicability of the proposed model was investigated in this study, it is still inadequate because of the lack of observed data. The proposed model can calculate trajectories of water particles at the vicinity of water surface which can easily observed. In the Go River confluences, water level gages have been set to obtain water surface profiles in the confluences. In addition to this, observations for the water surface velocities and its trajectories are planned to be conducted by using air photographs and GPS floats during floods. Based on these observed data, we advance the examination for the applicability of the model.

## 4 CONCLUSIONS

This study developed the numerical model capable of calculating the flood flows and bed variations in the confluences of rivers having a comparable drainage area by introducing the flux integral method considering a non-orthogonal direction of a grid line on the Bottom Velocity Computation (BVC) method.

The developed model was applied to the Oct. 1998 and Jun. 1999 floods of the Go river confluences, and its applicability and characteristics of flood flows and bed variations in the confluences were investigated together with the observed data. From the investigation, we clarified that the separation zones formed at the junction of rivers and flow convergence area affects the three-dimensional flow structures of their downstream.

## REFERENCES


Ashida, K. & Michiue, M. 1972. Study on hydraulic resistance and bed-load transport rate in alluvial streams, Proceedngs, JSCE, Vol. 206, pp. 59–69.

Fukuoka, S., Sato, H., Fujisawa, H. & Ohnuma, F. 2007. Assessment of permeability coefficient of vegetation and roughness coefficient under various floods and channel conditions, Annual Journal of Hydraulic Engineering, JSCE, Vol. 51, pp. 607–612.7.

Hirano, M. 1971. River-bed degradation with armoring, Proceedings, JSCE, Vol. 195, pp. 55–65.

Leonard B.P., MacVean M.K. & Lock A.P. 1994. The flux-integral method for multidimensional convection and diffusion, NASA Tech. Memo., pp. 333–342.

Miyawaki, S., Constantinescu, G., Rhoads, B. & Sukhodolov, A. 2010. Changes in three-dimensional flow structure at a river confluence with changes in momentum ratio, Proc. River Flow, Braunschweig, Germany.

Nakamura, T., Tanaka, R., Yabe, T. & Takizawa, K. 2001. Exactly Conservative Semi-Lagrangian Scheme for Multi-dimensional Hyperbolic Equations with Directional Splitting Technique, Journal of Computational Physics, Vol. 174, pp. 171–207, 2001.

Rhie, C.M. & Chow, W.L. 1983. Numerical study of the turbulent flow past an airfoil with trailing edge separation, AIAA Journal, Vol. 21, No.11, pp. 1525–1532.

Takizawa, K. & Yabe, T., 200. Development of Multi Dimensional Conservative Semi-Lagrangian Scheme, Symposium of numerical fluid dynamics, JSFM, Vol. 14, pp. 1–6.

Uchida, T. & Fukuoka, S. 2011. A bottom velocity computation method for estimating bed variation in a channel with submerged groins, Journal of JSCE, Ser. B1 (Hydraulic Engineering), Vol. 67, No.1, pp16–29, in Japanese.